


# Effect of Particle Size and Coke Formation on *n*-Octane Dehydrogenation

Tobias Prucker<sup>1,\*</sup>, Aliena Lamberty<sup>1</sup>, Johannes Thiessen<sup>1</sup>, Matthias König<sup>2</sup>, and Andreas Jess<sup>1</sup>

DOI: 10.1002/cite.202200054

 This is an open access article under the terms of the Creative Commons Attribution License, which permits use, distribution and reproduction in any medium, provided the original work is properly cited.



Supporting Information  
available online

The effect of particle size as well as of coke formation on conversion of intermediate chain length paraffins (C<sub>6</sub>–C<sub>9</sub>) to the corresponding olefins was investigated on a promoted Pt catalyst with the model substance *n*-octane. Increasing the particle size leads to pore diffusion limitations and thus to a reduction of the activity for paraffin conversion and of the octene selectivity caused by more pronounced formation of consecutive products (aromatics, octadienes). Both effects are adequately predicted by the developed kinetic model. The activity of dehydrogenation declines with the content of coke, but to a lesser extent than the rate of coke formation, which is beneficial regarding the catalyst lifetime. The initial activity is fully recovered by mild coke burn-off ( $T < 470$  °C).

**Keywords:** Catalyst deactivation, Internal diffusion limitation, Modeling, *n*-Octane dehydrogenation

*Received:* May 11, 2022; *accepted:* July 26, 2022

## 1 Introduction

The heterogeneously catalyzed dehydrogenation of linear alkanes to the corresponding monoolefins is of great interest for the production of alkenes with a specific chain length. While the dehydrogenation of short-chain (C<sub>2</sub>–C<sub>4</sub>) and long-chain paraffins (C<sub>10</sub>–C<sub>14</sub>) has been investigated thoroughly, studies regarding the conversion of *n*-paraffins with intermediate chain length (C<sub>6</sub>–C<sub>9</sub>) to linear olefins are rather scarce. In this context, we recently developed an alumina-supported Pt catalyst for dehydrogenation of paraffins with intermediate chain length by applying Sn, K, and Ce as promoter metals and adjusting their contents to achieve high olefin yields [1]. Furthermore, the reaction kinetics of the equilibrium-limited main dehydrogenation reaction of monoolefin formation as well as the accompanying formation of dienes and aromatics was investigated and modeled for the model substance *n*-octane [1]. The kinetic model was developed in the absence of mass transfer limitations by proper sizing of the catalyst particles ( $d_{\text{par}} < 188$  μm). Furthermore, a falsification of the kinetic parameters by deactivation due to coke formation was prevented by evaluation of the kinetic data at short experimental run times.

In an industrial application of the catalyst in a fixed-bed reactor, the reaction kinetics may be influenced by internal diffusion processes arising from the use of catalyst particles above a specific size, indispensable for a reduction of the pressure drop over the fixed bed. In addition, coke deposi-

tion on the (internal) catalytic surface leads to a decay of the catalyst activity with time. Consequently, this paper reports on the effect of particle size as well as of coke formation on the dehydrogenation of *n*-octane. While the effective kinetics were computed by modeling the interplay of internal diffusion and the intrinsic chemical reaction, the impact of carbonaceous deposits on the activity was investigated in a magnetic suspension balance allowing to determine the coke content and performance of the catalyst simultaneously.

## 2 Experimental

The measurements were performed in two different experimental setups. The catalyst was always pre-reduced in situ prior to reaction with 20 vol % H<sub>2</sub> in N<sub>2</sub> (10 K min<sup>-1</sup> to 435 °C with 60 min hold) and all measurements were con-

<sup>1</sup>Tobias Prucker, Aliena Lamberty, Dr.-Ing. Johannes Thiessen, Prof. Dr.-Ing. Andreas Jess  
tobias.prucker@uni-bayreuth.de  
University of Bayreuth, Department of Chemical Engineering, Universitätsstraße 30, 95447 Bayreuth, Germany.

<sup>2</sup>Dr. Matthias König  
Evonik Operations GmbH, Paul-Baumann-Straße 1, 45772 Marl, Germany.

ducted at ambient pressure. The catalyst, optimized for the dehydrogenation of paraffins with intermediate chain length, consists of 0.38 wt % Pt, 1.05 wt % Sn, 0.54 wt % K, and 0.70 wt % Ce supported on  $\text{Al}_2\text{O}_3$ . Details on catalyst preparation by wet impregnation can be found in [1] and important properties of the Pt catalyst are listed in Tab. S1 in the Supporting Information.

The effective kinetics were investigated in an electrically heated fixed-bed reactor equipped with an online GC (referred to as FBR setup; for details, see [1]). The spherical catalyst particles (2.5 mm diameter) were crushed and sieved to different sieve fractions leading to mean particle diameters  $d_{\text{par}}$  of 63, 94, 188, 325, 605, and 1300  $\mu\text{m}$ . The data was obtained in the absence of catalyst deactivation (evaluation at 15 min time on stream (TOS);  $p_{\text{H}_2} \geq 0.6$  bar). Further details regarding the experimental procedure and conditions are given in the Supporting Information.

The effect of coke formation on the dehydrogenation was studied in a second setup (referred to as MSB setup) with a magnetic suspension balance (MSB, Rubotherm) as reactor, allowing for in situ determination of the change of catalyst mass by coke formation and the simultaneous measurement of the catalyst activity. The deactivation experiments were conducted with particles of 188  $\mu\text{m}$  diameter to exclude intraparticle transport limitations [1]. The whole installation (Fig. 1) includes two mass flow controllers (Bronkhorst) for dosing of  $\text{H}_2$  and  $\text{N}_2$  (as balance), a tempered saturator filled with *n*-octane (Alfa Aesar), the MSB, and a cold trap ( $-79^\circ\text{C}$ ) for sampling (subsequent analysis in a GC). Three-way valves enable bypassing of the saturator (for catalyst reduction) or the MSB. The whole piping between the saturator and sampling is heated to  $120^\circ\text{C}$  to prevent hydrocarbon condensation. The experiments were conducted with a  $\text{N}_2$ - $\text{H}_2$  volume flow of  $10 \text{ L}_\text{N} \text{ h}^{-1}$  (273.15 K, 1013.25 hPa) at an initial *n*-octane partial pressure of 0.1 bar. The  $\text{H}_2$  partial pressure was varied between 0.3 and 0.6 bar to determine the influence of hydrogen on the coke

formation rate. Further details regarding the measurements with the MSB setup are given in the Supporting Information.

The experimental data obtained in the MSB as well as in the FBR setup were evaluated based on the GC peak areas. The *n*-octane conversion  $X_p$  as well as the product selectivities  $S_i$  and yields  $Y_i$  of *n*-octenes, *n*-octadienes, and aromatics (grouped to pseudospecies) were calculated according to Eqs. (1) to (3).

$$X_p = \frac{A_{\text{tot}} - A_p}{A_{\text{tot}}} \quad (1)$$

$$S_i = \frac{A_i}{A_{\text{tot}} - A_p} \quad (2)$$

$$Y_i = S_i X_p \quad (3)$$

$A_{\text{tot}}$  denotes the total peak area and  $A_i$  the area of the respective pseudospecies  $i$ . The partial pressures of the different product groups were obtained by Eq. (4).

$$p_i = Y_i p_p \quad (4)$$

The modified residence time  $\tau_m$  was defined according to Eq. (5) as the ratio of catalyst mass  $m_{\text{cat}}$  to the total molar feed flow rate  $\dot{n}_{\text{tot}}$  (calculated by the ideal gas law).

$$\tau_m = \frac{m_{\text{cat}}}{\dot{n}_{\text{tot}}} = \frac{m_{\text{cat}} T_{\text{norm}} R}{\dot{V}_{\text{tot, norm}} p_{\text{norm}}} \quad (5)$$

However, in case of the MSB setup, it could not be avoided that a certain ratio of the feed flow (depending on the pressure drop of the catalyst bed) bypassed the catalyst bed at the bearing point of the flow-through cell. Consequently, the true residence time was estimated by comparison of the experimental conversion and the expected value according to the intrinsic kinetic model from [1].

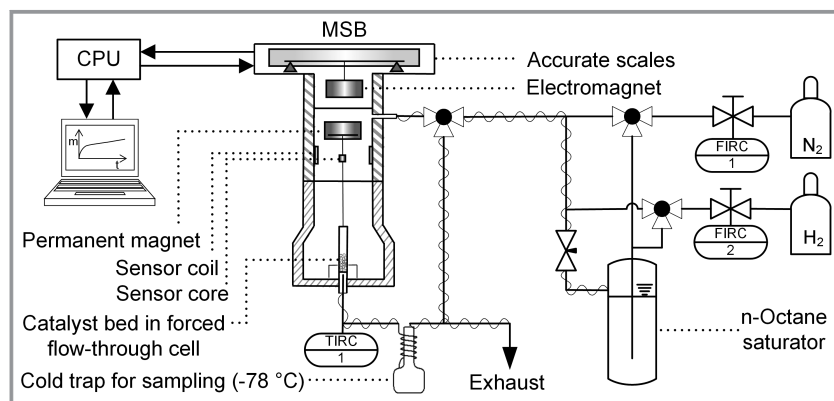


**Figure 1.** Simplified scheme of the MSB setup for the simultaneous determination of the catalyst mass gain by coke formation and catalytic activity during *n*-octane dehydrogenation. FIRC, flow indicating recording controlling; TIRC, temperature indicating recording controlling; MSB, magnetic suspension balance; CPU, central processing unit.

## 3 Calculations and Modeling

### 3.1 Modeling of the Effective Kinetics

To transfer the intrinsic kinetic model to industrially relevant catalyst sizes, the interplay of internal diffusion processes and chemical reactions was included. The catalyst particles are assumed to be spherical and considered isothermal just as the catalyst bed. Volume changes by the formation of  $\text{H}_2$  could be neglected due to the low conversion and the rather small paraffin partial pressure. In Fig. 2, the modeling methodology applied is schematically shown.

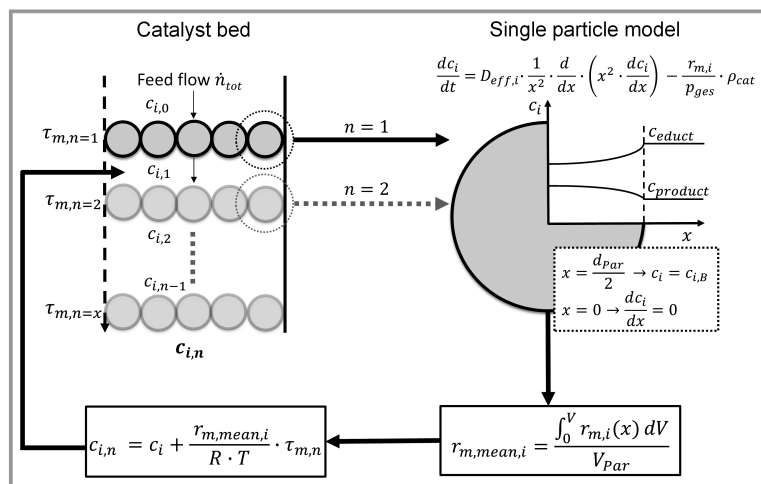


**Figure 2.** Schematic representation of the numerical calculation procedure of the reactant concentrations or partial pressure in dependency of the modified residence time.

The complete model consists of two parts. In the first part (single particle model), the concentration or partial pressure profiles of each reactant  $i$  within the catalyst particle are computed. This is achieved by numerically solving Eq. (6) (Matlab; pdepe), which describes the mass balances of each species  $i$  over an infinitesimally small catalyst volume.

$$\frac{dc_i}{dt} = D_{\text{eff},i} \frac{1}{x^2} \frac{d}{dx} \left( x^2 \frac{dc_i}{dx} \right) - \frac{r_{m,i}}{\rho_{\text{ges}}} \rho_{\text{cat}} \quad (6)$$

As boundary conditions, the local symmetry condition

$$\left. \frac{dc_i}{dx} \right|_{r=0} = 0 \quad (7)$$

and the concentration at the particle surface

$$c_i|_{r=R} = c_{i,s} \quad (8)$$

are used. Since external diffusion limitation can be excluded (Supporting Information), the surface concentration  $c_{i,s}$  equals the known bulk concentration  $c_{i,B}$ .

In the second part of the complete model, the results from the single particle model are transferred to an integral catalyst bed. For this purpose, the catalyst bed is divided into  $n$  imaginary layers. Each layer, comprising a known number of catalyst particles with a specific mean diameter, corresponds to a certain modified residence time  $\tau_{m,n}$ , depending on the chosen feed flow  $\dot{n}_{\text{tot}}$ .

At first, the single particle model is solved for the initial feed concentrations ( $\tau_m = 0$ ) to obtain the partial pressure profiles within the particles of layer  $n = 1$ . The partial pressures are used to determine the radius-dependent reaction rates via the known intrinsic kinetics within the particles of layer  $n = 1$ , corresponding to the modified residence time  $\tau_{m,1}$  [1]. The reaction rates of each species  $i$   $r_{m,i}(x)$  in the

first layer of the catalyst bed are averaged over the catalyst volume.

$$r_{m,\text{mean},i} = \frac{\int_0^V r_{m,i}(x) dV}{V_{\text{Par}}} \quad (9)$$

Thereby, the concentrations behind the first catalyst layer  $c_{i,1}$  can be obtained by

$$c_{i,1} = c_{i,0} + \frac{r_{m,\text{mean},i}}{RT} \tau_{m,1} \quad (10)$$

Now the single particle model is solved again for the new bulk concentrations  $c_{i,1}$  to determine the partial pressure profiles and mean reaction rates of particles in the second layer  $n = 2$ , allowing to compute the concentrations behind this second layer  $c_{i,2}$ . This procedure is repeated until the desired residence time  $\tau_m = \sum_n \tau_{m,n}$  is reached.

The effective diffusion coefficients  $D_{\text{eff},i}$  of each species  $i$  within the pore structure of the catalyst were described by the random pore model [2] as described in detail in the Supporting Information. Note that the catalyst exhibits intrusions (Fig. S2) with an unknown diameter, which were treated as macropores in the model with the mean diameter as an adjustable model parameter (Tab. S1).

### 3.2 Numerical Determination of Catalyst Activity

To achieve a satisfactorily coke mass resolution in the MSB at the rather low amounts of coke formed ( $< 2.7$  wt %), 100 mg of catalyst were used. Under the applied conditions, the reactor was thus operated in an integral way ( $20\% < X_p < 30\%$ ). Since the coke content in an integral reactor may change with the position in the fixed bed, measurements under integral conditions only give rise to a mean coke content. The latter does not necessarily correlate with the mean activity of the catalyst bed [3]. However, in the particular case of  $n$ -octane dehydrogenation, the change of coke content with the bed length is small (Fig. S3). The location-dependent values do not deviate more than 15% from the accessible average coke content of the catalyst bed, allowing to correlate the mean coke content with the catalyst activity of  $n$ -octane dehydrogenation, even though the partial pressures in the reactor cannot be considered gradientless, but the axial gradients of the concentrations of all compounds are still rather small.

The coke formed on the catalyst leads to a reduction of the apparent  $n$ -octane reaction rate with TOS. However, the rate is also influenced by the thermodynamic driving force and the product inhibition by the formed  $n$ -octenes, which both change in the course of the experiment due to the decreasing conversion induced by coke formation. Thus, the activity decline in the integral reactor cannot be expressed by a normalized apparent  $n$ -octane reaction rate

$r_P(t)/r_{P,\text{initial}}$  (Fig. 6), but had to be determined numerically with the intrinsic kinetic model to account for the mentioned effects. Thus, an activity parameter  $a_P$  was introduced into the rate equation for paraffin conversion, according to Eq. (11).

$$\frac{dp_P}{d\tau_m} = a_P \frac{-k_{m,1} \left( p_P - \frac{f_{PM} p_{H_2}}{K_{p,PM} p_{\text{norm}}} \right)}{(1 + K_{\text{ads},M} f_{PM})^2} \quad (11)$$

The whole set of ODEs describing the reaction network (Tab. S2) was integrated numerically in Matlab (ode15s) to compute the expected partial pressures in the absence of deactivation. The catalyst activity was then determined by fitting  $a_P$  to the experimental partial pressures of  $n$ -octane  $p_P$  and  $n$ -octenes  $p_M$  (Matlab; fmincon) by means of the following objective function:

$$f(\tau_m) = \left( \frac{p_{P,\text{mod}}(a_P) - p_{P,\text{exp}}(a_P)}{p_{P,\text{exp,max}}} \right)^2 + \left( \frac{p_{M,\text{mod}}(a_P) - p_{M,\text{exp}}(a_P)}{p_{M,\text{exp,max}}} \right)^2 \quad (12)$$

To investigate the influence of coke on the coke formation, the time-dependent coke contents from the MSB were fitted empirically (solid lines in Fig. 6 and S4a) and the rates of coke formation  $r_C$  were obtained from the time derivatives of these fits (Fig. S4b).

## 4 Results

### 4.1 Results in the Absence of Catalyst Deactivation – Effective Reaction Kinetics

The basis for modeling the particle size effect is the recently published intrinsic kinetic model. It describes the chemical reaction rates of  $n$ -octane dehydrogenation as well as of the accompanying reactions without influence of diffusion over the non-deactivated catalyst and will be shortly summarized in the following (for details, see [1]). The applied reaction network is shown in Fig. 3a and includes the consecutive dehydrogenation of  $n$ -octenes to  $n$ -octadienes, which are partially further converted to  $C_8$  aromatics [4–6]. The kinetic analysis revealed that the thermodynamic equilibrium between  $n$ -octenes and  $n$ -octadienes is nearly instantaneously established at the given reaction conditions. Thus, mono- and diolefins are clustered and the formation of their blend is simplistically described by a single rate equation. The proportion of each olefinic compound in this blend is

accessible by the experimental equilibrium constant of  $n$ -octene dehydrogenation  $K_{p,MD}$ , deduced from the experimental data, since no thermodynamic data were available. The equilibrium constant of  $n$ -octane dehydrogenation  $K_{p,PM}$  was calculated by the software CHEMCAD (version 7.1.5). Furthermore, the derived rate equation for  $n$ -octane conversion considers the inhibiting effect of  $n$ -octene adsorption on the dehydrogenation rate. This intrinsic kinetic model predicts the hydrocarbon distribution, e.g., the influence of residence time, accurately (Fig. 3b). The full set of differential equations can be found in [1] and/or in the Supporting Information (Tab. S2) along with the model parameters (Tab. S3).

This intrinsic kinetic model was expanded according to the methodology outlined before (Sect. 3.1) by inclusion of internal diffusion processes. In Fig. 4a, the effect of particle size on the hydrocarbon distribution is depicted for otherwise constant reaction conditions. As expected, the amount of desired  $n$ -octenes decreases with increasing particle diameter due to pore diffusion resistance and thus a lower effective reaction rate. Consequently, the partial pressure of  $n$ -octadienes, which is directly coupled to the partial pressure of  $n$ -octenes by the experimental  $K_{p,MD}$ , decreases similarly. The measured selectivity to the intermediate  $n$ -octenes decreases from 87 % (at  $X_P = 15\%$ ) in the intrinsic case ( $d_{\text{par}} \leq 188 \mu\text{m}$ ) to 74 % at an  $n$ -octane conversion of 11.4 % when using particles with a diameter of 1.3 mm. For details on the selectivity data, see Fig. S5. The mentioned effects of the particle size are more pronounced at higher temperatures due to the strong increase of the chemical reaction rate (constant) compared to the rather

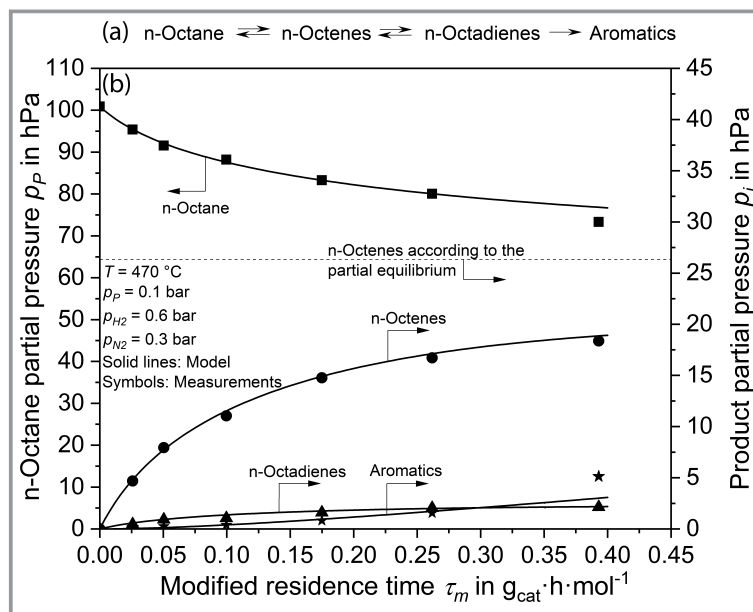


**Figure 3.** a) Simplified reaction scheme for  $n$ -octane dehydrogenation utilized for modeling of the reaction kinetics [4]. b) Influence of the modified residence time on the hydrocarbon distribution in the dehydrogenation of  $n$ -octane in the absence of pore diffusion limitation and catalyst deactivation ( $d_{\text{par}} \leq 188 \mu\text{m}$ ).

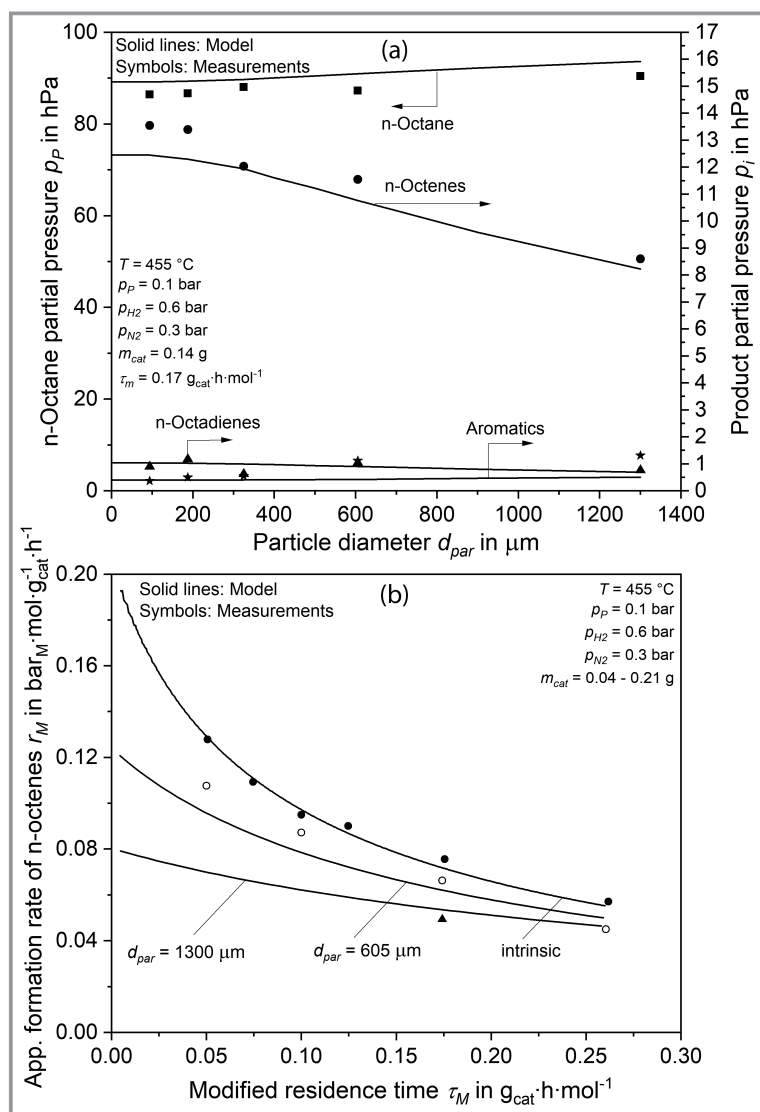


**Figure 4.** a) Modeled and measured particle size effect on the hydrocarbon distribution in the dehydrogenation of *n*-octane. b) Influence of the modified residence time on the apparent monoolefin formation rate at different particle sizes.

small increase of the diffusion rate (coefficient) and are also well described by the model (Fig. S6).

Besides temperature, the degree of diffusion limitation strongly depends on the position in the catalyst bed. Fig. 4b shows the apparent *n*-octene formation rate  $r_M$  for three particle diameters of 188 (intrinsic), 605, and 1300  $\mu\text{m}$  vs the modified residence time. The higher the latter, the smaller the distance to the partial equilibrium between octane and octenes, and thus  $r_{M,eff}$ . As a consequence, the formation rates for different particle sizes converge at high residence times, as the equilibrium is then more and more approached.

Fig. 5a shows the calculated radial partial pressure profiles inside catalyst particles of 605  $\mu\text{m}$  diameter at two modified residence times corresponding to the in- and outlet of the

catalyst bed. Although the depicted partial pressure changes, especially of octane, seem rather small, they have a distinct influence on the rate of octene formation. Even at the inlet of the catalyst bed, the partial pressure of *n*-octenes in the particle center reaches 50 % of the equilibrium value (Fig. 5a, right arrow). Consequently, the hydrogenation rate of octenes to octane as well as the inhibiting effect of octenes on the formation rate  $r_M$  strongly increase while approaching the particle center. This leads to a strong decrease of the effective rate of octene formation towards the center of the catalyst particle, as can be seen in Fig. 5b.

The stated strong influence of pore diffusion at industrially relevant particle sizes along with the problem of a high pressure drop over the catalyst bed at small catalyst sizes may be overcome by design of a core-shell catalyst, which, however, requires further research, which was out of the scope of this study.

## 4.2 Catalyst Deactivation by Coke Formation

Besides diffusion processes, the formation of coke influences the dehydrogenation rate. In Fig. 6, the decline of the normalized apparent *n*-octane reaction rate and the numerically determined activity  $a_P$  (Sect. 3.2) are presented, along with the simultaneously obtained mass gain of the catalyst by coke formation. All data on deactivation were obtained in absence of mass transport limitations ( $d_{par} = 188$   $\mu\text{m}$ ).

The deactivation process can be roughly divided into two parts with respect to TOS, a quick deactivation within the first 500 min of reaction, which is governed by a fast coke deposition, and a second slower coke formation stage with a corresponding moderate activity decline. Caused by the decreasing *n*-octane conversion, the driving force for the reaction rate, which is the distance to the thermodynamic equilibrium composition, increases in the course of the experiments. Furthermore, the amount of formed *n*-octenes decreases and thus their inhibiting effect on the dehydrogenation rate. Consequently, the decline in the normalized *n*-octane reaction rate is lower than that of the actual catalyst activity  $a_P$ , as can be seen from the graphs in Fig. 6. Or in other words: part of the catalyst deactivation with respect to the overall dehydrogenation rate in a catalyst bed is compensated by the increasing driving force and decreasing product inhibition.

Following the approach of Froment [7], the coke and activity vs time data of all MSB experiments were used to derive the dependency of the dehydrogenation activity  $a_P$

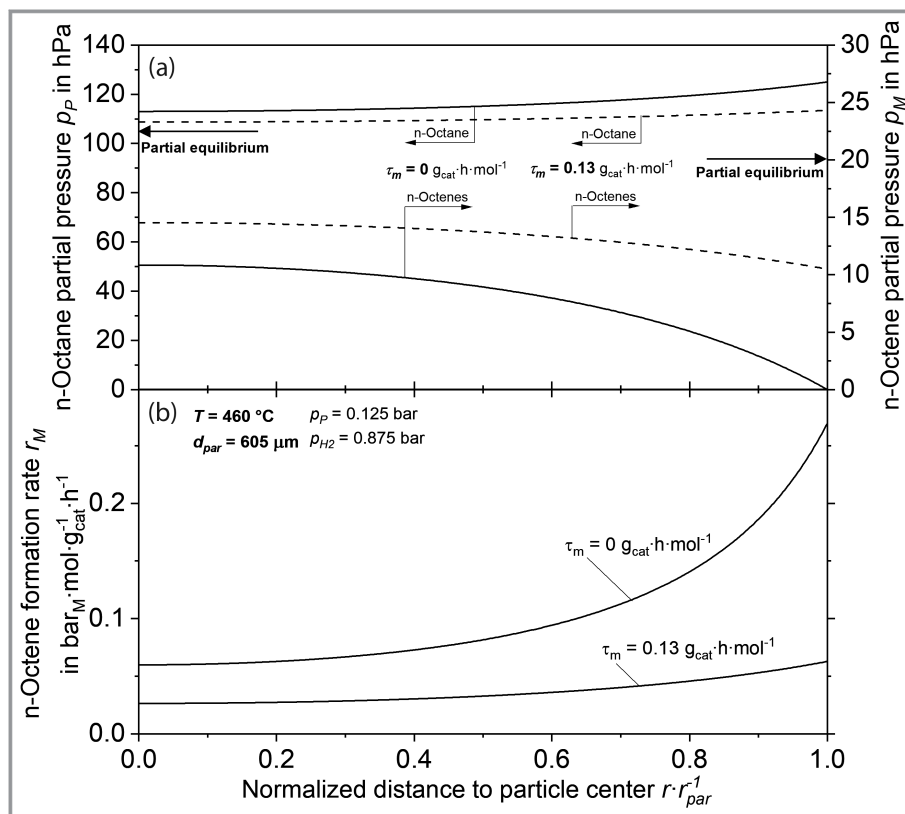


**Figure 5.** a) Simulated partial pressure profiles of *n*-octane and *n*-octenes inside a catalyst particle at two different modified residence times corresponding to the start and the end of the catalyst bed. Note that for the sake of clarity, the partial pressures of *n*-octadienes and aromatics are not presented. b) Corresponding formation rates of octenes inside the catalyst.

from the coke content  $C_c$  (Fig. 7). It is remarkable that the deactivating effect of the coke decreases with increasing coke content. The dehydrogenation activity was empirically

interact the loss of activity by coke formation, the initial activity needs to be restored by continuous catalyst regeneration. Therefore, it was shown for seven consecutive coking-

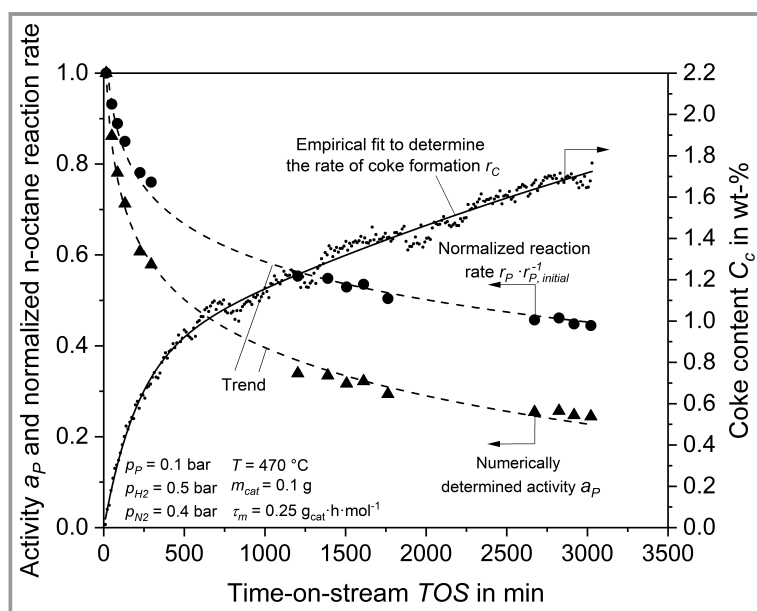


**Figure 6.** Coke content in dependency of TOS and catalyst activity of the *n*-octane dehydrogenation reaction expressed in terms of the flawed normalized paraffin reaction rate as well as by the numerically determined activity  $a_P$ .

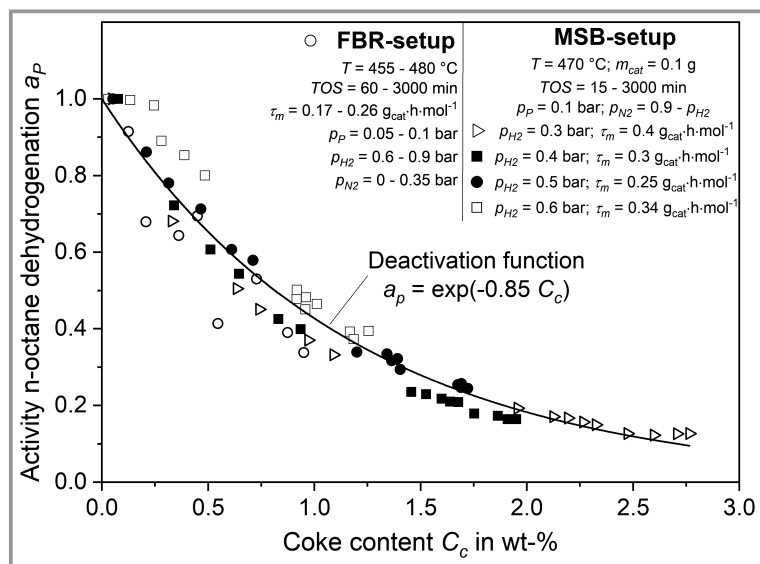


**Figure 7.** Influence of the catalyst coke content on its activity in the dehydrogenation of *n*-octane.

regeneration cycles that the catalyst activity can be nearly fully recovered by coke combustion under mild regeneration conditions of 470 °C and 1 vol % O<sub>2</sub> in N<sub>2</sub> (Fig. S7).

Thus far, the deactivation behavior of the main *n*-octane dehydrogenation reaction was analyzed. However, the deposited coke may also influence accompanying reactions, namely, the dehydrogenation of *n*-octenes, the formation of aromatics, and the coke formation itself, which will be discussed below.

According to the kinetic analysis in the absence of catalyst deactivation [1], the formed amount of *n*-octadienes from *n*-octenes is practically only governed by thermodynamics (very fast reaction) and thus only determined by the equilibrium constant  $K_{p,MD}$ . This assumption seems to be valid for coke contents up to approximately 1.7 wt %, as depicted in Fig. S8. Below this threshold value, the dehydrogenation of *n*-octenes is so fast that the expected equilibrium composition is reached in good approximation. At higher coke contents, the *n*-octene dehydrogenation rate declines to such an extent that a deviation of the *n*-octadienes' partial pressure from the expected equilibrium pressure occurs. As expected, this deviation increases with rising coke content due to the advancing deactivation. The catalyst activity for the formation of aromatics  $a_A$  was determined analogically to the procedure outlined in Sect. 3.2 (for the calculation of *n*-octane dehydrogenation activity) by introducing the activity  $a_A$  in the rate equation for the formation of aromatics (Tab. S2, Eq. (S3)) and fitting of the latter to the experimental data. However, no systematic relation between  $a_A$  and the coke content could be observed. A possible cause for this could be the generally low partial pressure of *n*-octadienes (precursor for aromatics) as well as of the aromatics (compare Fig. 3 or Fig. 4a) in the product mixture leading to a relative high

uncertainty in the modeled as well as experimental formation rate of aromatics and thus in the numerically determined activity  $a_A$ .

The catalyst coke formation activity  $a_C$  in dependency of the coke content is depicted in Fig. 8. The deactivation function of the *n*-octane dehydrogenation reaction is additionally given (solid line) for comparison. At a low coke content, here below approximately 0.5 wt %, the decline of the coke formation rate  $r_C$  proceeds analogically to the decrease of the activity of paraffin dehydrogenation  $a_p$ . But at a higher coke content, the coke formation rate decreases faster with increasing  $C_C$  than the activity of the main reaction. Furthermore, the decline of  $r_C$  proceeds more readily at higher H<sub>2</sub> partial pressures. H<sub>2</sub> is known to be capable to remove carbonaceous deposits from Pt catalysts by hydrogenation or by suppressing the formation of coke precursors such as unsaturated hydrocarbons as shown, e.g., for Pt-Sn/Al<sub>2</sub>O<sub>3</sub> catalysts after coking with *n*-hexane [11] or for a Pt/Al<sub>2</sub>O<sub>3</sub> reforming catalyst coked with hydrogen-diluted cyclohexane [12]. The measurable net coke formation rate  $r_C$  in a H<sub>2</sub>-containing atmosphere may thus be composed of a coke formation rate superimposed to a coke removal rate [12, 13]. The faster decline of  $r_C$  at higher H<sub>2</sub> partial pressure may consequently not be caused by a quicker catalyst deactivation but by a reduction of the measurable net formation rate  $r_C$  due to an intensified coke removal from the catalyst surface at higher H<sub>2</sub> partial pressures.

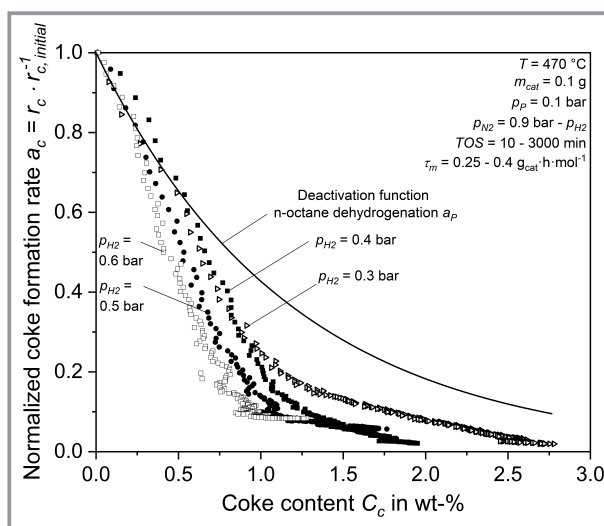


**Figure 8.** Effect of the coke content on the decline of the coke formation rate  $r_C$  at different H<sub>2</sub> partial pressures in the absence of mass transport limitations ( $d_{\text{par}} < 188 \mu\text{m}$ ). The deactivation function of paraffin conversion (solid line) is additionally presented for comparison.

## 5 Conclusion

The effect of internal mass transport limitations on the *n*-octane dehydrogenation performance of a Pt-Sn catalyst was investigated. An increase of the particle size from below 188  $\mu\text{m}$  (no mass transport limitations) to industrially relevant particle sizes ( $d_{\text{par}} = 1.3 \text{ mm}$ ) leads to a decrease of the octene yield caused by a lower conversion and a more pronounced formation of unwanted consecutive products. The hydrocarbon distribution predicted by the developed model, which couples pore diffusion with the intrinsic reaction kinetics, is in good accordance with the experimental data. The drawbacks caused by internal diffusion limitations may be overcome by the use of a core-shell catalyst, which, however, requires further research.

The influence of coke formation on the main dehydrogenation reaction and the rate of coke formation itself was studied in a magnetic suspension balance. The dependency of the dehydrogenation activity on the amount of coke could be well correlated empirically with an exponential decay function. The rate of coke formation in a  $\text{H}_2$ -containing atmosphere declines stronger with respect to the coke content than the activity of the main reaction, which is beneficial for a prolonged catalyst lifetime.

## Supporting Information

Supporting Information for this article can be found under DOI: <https://doi.org/10.1002/cite.202200054>. This section includes additional references to primary literature relevant for this research [14–19].

The authors thank Evonik Operations GmbH for financial support. Open access funding enabled and organized by Projekt DEAL.

## Symbols used

$a$	[-]	catalyst activity
$A$	[V s]	GC peak area
$c$	[mol s <sup>-3</sup> ]	concentration
$C_c$	[-]	coke content
$d$	[m]	diameter
$D$	[m <sup>2</sup> s <sup>-1</sup> ]	diffusion coefficient
$K_{\text{p,MD}}$	[-]	equilibrium constant of the dehydrogenation of octenes to octadienes
$K_{\text{p,PM}}$	[-]	equilibrium constant of the dehydrogenation of <i>n</i> -octane to <i>n</i> -octenes
$m$	[kg]	mass
$\dot{n}$	[mol s <sup>-1</sup> ]	molar flow
$p$	[Pa]	partial pressure

$r$	[bar s <sup>-1</sup> g <sub>cat</sub> <sup>-1</sup> ]	reaction rate
$S$	[-]	selectivity
$t$	[s]	time
$T$	[°C, K]	temperature
$\dot{V}$	[m <sup>3</sup> s <sup>-1</sup> ]	volume flow
$X$	[-]	conversion
$Y$	[-]	yield

## Greek letter

$\tau_m$	[g <sub>cat</sub> h mol <sup>-1</sup> ]	modified residence time
----------	---	-------------------------

## Sub- and superscripts

eff	effective
$i$	compound $i$ ( <i>n</i> -octane (P), <i>n</i> -octenes (M), <i>n</i> -octadienes (D), aromatics (A))
par	particle
tot	total

## Abbreviations

FBR	fixed-bed reactor
GC	gas chromatograph
MSB	magnetic suspension balance
TOS	time-on-stream

## References

- [1] T. Prucker, A. Lamberty, J. Thiessen, M. König, A. Jess, *Chem. Eng. J.* **2022**, *442*, 136233. DOI: <https://doi.org/10.1016/j.cej.2022.136233>
- [2] N. Wakao, J. M. Smith, *Chem. Eng. Sci.* **1962**, *17* (11), 825–834. DOI: [https://doi.org/10.1016/0009-2509\(62\)87015-8](https://doi.org/10.1016/0009-2509(62)87015-8)
- [3] H. C. Beirnaert, R. Vermeulen, G. F. Froment, *Stud. Surf. Sci. Catal.* **1994**, *88*, 97–112. DOI: [https://doi.org/10.1016/S0167-2991\(08\)62732-9](https://doi.org/10.1016/S0167-2991(08)62732-9)
- [4] M. M. Bhasin, J. H. McCain, B. V. Vora, T. Imai, P. R. Pujadó, *Appl. Catal., A* **2001**, *221* (1–2), 397–419. DOI: [https://doi.org/10.1016/S0926-860X\(01\)00816-X](https://doi.org/10.1016/S0926-860X(01)00816-X)
- [5] G. Padmavathi, K. K. Chaudhuri, D. Rajeshwer, G. S. Rao, K. R. Krishnamurthy, P. C. Trivedi, K. K. Hathi, N. Subramanyam, *Chem. Eng. Sci.* **2005**, *60* (15), 4119–4129. DOI: <https://doi.org/10.1016/j.ces.2005.01.039>
- [6] S. He, D. Castello, K. R. Krishnamurthy, A. S. Al-Fatesh, J. G. M. Winkelman, K. Seshan, A. H. Fakeeha, S. R. A. Kersten, H. J. Heeres, *Appl. Catal., A* **2019**, *579*, 130–140. DOI: <https://doi.org/10.1016/j.apcata.2019.04.026>
- [7] G. F. Froment, *Stud. Surf. Sci. Catal.* **1991**, *68*, 53–83.
- [8] R. P. De Pauw, G. F. Froment, *Chem. Eng. Sci.* **1975**, *30* (8), 789–801. DOI: [https://doi.org/10.1016/0009-2509\(75\)80043-1](https://doi.org/10.1016/0009-2509(75)80043-1)
- [9] F. J. Dumez, G. F. Froment, *Ind. Eng. Chem. Process Des. Dev.* **1976**, *15* (2), 291–301. DOI: <https://doi.org/10.1021/i260058a014>
- [10] S. He, C. Sun, X. Yang, B. Wang, X. Dai, Z. Bai, *Chem. Eng. J.* **2010**, *163* (3), 389–394. DOI: <https://doi.org/10.1016/j.cej.2010.07.024>



- [11] K. Matusek, C. Kappenstein, M. Guérin, Z. Paál, *Catal. Lett.* **2000**, *64* (1), 33–36. DOI: <https://doi.org/10.1023/A:1019026701636>
- [12] J. Biswas, P. G. Gray, D. D. Do, *Appl. Catal.* **1987**, *32*, 249–274. DOI: [https://doi.org/10.1016/S0166-9834\(00\)80629-6](https://doi.org/10.1016/S0166-9834(00)80629-6)
- [13] N. M. Ostrovskii, *Kinet. Catal.* **2001**, *42* (3), 326–333. DOI: <https://doi.org/10.1023/A:1010457114059>
- [14] A. Jess, P. Wasserscheid, *Chemical Technology*, 2nd ed., Wiley-VCH, Weinheim **2020**.
- [15] B. E. Poling, J. M. Prausnitz, J. P. O'Connell, *The Properties of Gases and Liquids*, 5th ed., McGrawHill, New York **2001**.
- [16] E. N. Fuller, P. D. Schettler, J. C. Giddings, *Ind. Eng. Chem.* **1966**, *58* (5), 18–27. DOI: <https://doi.org/10.1021/ie50677a007>
- [17] E. N. Fuller, K. Ensley, J. C. Giddings, *J. Phys. Chem.* **1969**, *73* (11), 3679–3685. DOI: <https://doi.org/10.1021/j100845a020>
- [18] G. F. Froment, K. B. Bischoff, J. De Wilde, *Chemical Reactor Analysis and Design*, 3rd ed., John Wiley & Sons, Hoboken, NJ **2010**.
- [19] H. Giesche, *Part. Part. Syst. Charact.* **2006**, *23* (1), 9–19. DOI: <https://doi.org/10.1002/ppsc.200601009>